INTERNATIONAL JOURNAL FOR NUMERICAL METHODS IN FLUIDS, VOL. 4, 25–41 (1984)

NUMERICAL MODELLING OF WIND FLOW OVER BUILDINGS IN TWO DIMENSIONS

T. HANSON, D. M. SUMMERS AND C. B. WILSON

Department of Architecture, University of Edinburgh, 20 Chambers Street, Edinburgh EH1 1JZ, Scotland

SUMMARY

Numerical solutions to the Navier–Stokes equation may provide designers with predictions of the wind environment of buildings under design. To investigate this possibility, two complementary solution procedures are implemented for two-dimensional geometry: a random vortex method to depict the flow evolution, and a control volume method to depict the steady flow field. These are both illustrated by specific application to the case of a building form with a roof of arbitrary pitch.

KEY WORDS Architectural Wind-flow Environmental Problems Random Vortex Method Control Volume Method

INTRODUCTION

The quality of architectural and urban design can be improved by some assessment of the consequences of a proposed building for its wind environment. Ideally such an assessment should inform the design from its inception.[1] At any stage it should provide some description of a building's wind micro-climate and an estimate of the implications of this both for the building's energy performance and for human comfort in the surrounding urban space. For such a procedure to be useful to a designer it ought to be reasonably accessible and immediate and it ought to be sufficiently versatile to accommodate groups of buildings of some geometrical complexity.

The wind environment of proposed buildings has usually been studied in the past by scale-model experiments in wind-tunnels. The execution of such experiments is seldom immediate since they require access to a wind-tunnel and to the expertise of wind-tunnel personnel. Of course, protraction of the design process is usually expensive: in the context of architectural practice there has been little commercial incentive to take any detailed interest in problems related to the wind environment. The expense and experimental difficulty which attend wind-tunnel modelling suggest that a computer simulation of wind flow around built form could be of advantage as an alternative (and complementary) approach to the problem.

The numerical calculations associated with wind flow around buildings require the solution of the Navier–Stokes equation for the case of slightly viscous flow around large-scale bluff bodies. This is therefore a problem characterized by high Reynolds number (typically Re is of order 10^6) and by a flow field which is sharply separated and which is normally turbulent.

The surface boundary layer on the building itself will have thickness of order $Re^{-1/2}$ and is typically some centimetres thin. If numerical solution is to be effected by approximating the differential equation by its equivalent difference equations, then an ideal grid configuration would have to encompass the detail of this boundary layer as well as the full expanse of the developed flow. In many engineering contexts it is difficult to contrive a configuration which leads to a solution both computationally efficient and acceptably accurate.

0271–2091/84/010025–17$01.70

Received 9 June 1982
Revised 20 October 1982

Therefore we may ask: what accuracy would be acceptable in a numerical scheme to assess the wind environment of a proposed building? Various comparisons have been reported between measurements from scale-model wind-tunnel experiments and measurements from corresponding *in situ* full-scale experiments: these would suggest that the wind-tunnel can simulate the wind environment to within 20 per cent accuracy.[2,3] Thus we must expect at least this level of accuracy if a numerical flow solution is to be acceptable.

The computations required for structural loading calculations—as distinct from those for environmental problems—may require a level of accuracy more stringent than 20 per cent. We shall confine our attention here to the wind environment of a building, although we also briefly allude to the possible application of numerical techniques to problems of wind loading.

We have investigated two numerical methods for solving the Navier–Stokes equation (for two dimensional geometry) which provide plausible, stable solutions at high Reynolds number. The solutions obtained from these methods appear to be in qualitative agreement with each other and with wind-tunnel experiments. The claims of the originators of both methods would suggest to us that the formal accuracy of either method meets our requirements for the construction of a design tool.

NUMERICAL METHODS

Two quite different numerical methods suggest themselves for this problem: the random vortex method developed by Chorin[4–6] and a control volume method[7,8] which has been applied to an environmental problem by Caretto *et al.*[9] We shall describe both methods briefly.

The random vortex method

Reviews of vortex methods are to be found in References 10 and 11. Chorin's method has in common with other vortex methods the grid-free representation of flow dynamics in terms of discrete vortices.

The incompressible flow of a slightly viscous fluid around a bluff body can be often characterized by three flow regimes: away from the body the flow may be largely irrotational and may be thus formulated in terms of potential theory; in the immediate neighbourhood of solid surfaces a boundary layer is formed; beyond this boundary layer and in the downstream wake of the obstacle there is formed a region of concentrated vorticity which has been generated by the viscous interaction of the fluid with the obstacle. Vortex methods seek to approximate this entire flow field by considering it to consist everywhere of a superposition of an inviscid irrotational flow together with a flow induced by the fluid's distributed vorticity. To achieve this numerically, the vorticity is discretized and the evolution of the flow is accomplished by the fact that, so far as their inviscid motion is concerned, point vortices convect in the local velocity field. Thus, as time progresses, the vorticity redistributes itself and the corresponding velocity field induced by this vorticity will also evolve in time.

The fact that the method is grid-free is of particular importance. When a mesh is imposed on the solution domain and equivalent difference equations are posed for the Navier–Stokes equation, then the order of this numerical approximation can be the same as that of the viscous diffusion term in the equation. This gridding of the domain has the effect of introducing artificial viscosity into the computation. Chorin, on the other hand, represents the diffusive contribution to the motion of a discrete vortex by imparting to it after each time

interval dt a Gaussian random displacement (η_x, η_y) with zero mean and standard deviation $(2\,dt/Re)^{1/2}$; this is in analogy with Einstein's stochastic treatment of Brownian motion. The error associated with this representation lies in the approximation of the interaction between discrete vortices, and this should be an 'inviscid error' which does not depend functionally on Reynolds number.[6]

The nature of this approximation can be described in the specific context of a wind flow past a two-dimensional bluff body resting on the surface of the semi-infinite half-space occupying $y<0$ of the (x, y) plane. Outside the boundary layer of the surface of the obstacle (which is to be treated separately) the Navier–Stokes equation is expressed in dimensionless form in terms of scalar vorticity ξ and the velocity field $\mathbf{u}=(u, v)$ by

$$\frac{\partial \xi}{\partial t}+(\mathbf{u}\,.\,\nabla)\xi = Re^{-1}\nabla^2\xi \tag{1}$$

So far as the inviscid component of flow is concerned, we can relate vorticity to a stream function ψ by

$$\nabla^2\psi = -\xi \tag{2}$$

The velocities can then be determined as

$$\mathbf{u}=(u, v)=\left\{\frac{\partial \psi}{\partial y}, -\frac{\partial \psi}{\partial x}\right\} \tag{3}$$

The boundary conditions to be satisfied at solid surfaces consist of the impermeability condition

$$\mathbf{u}\,.\,\mathbf{n}=0 \tag{4}$$

and the condition of no-slip,

$$\mathbf{u}\,.\,\mathbf{s}=0 \tag{5}$$

($\mathbf{n}$ and $\mathbf{s}$ are unit vectors respectively normal and tangential to the solid surface). The solution to equation (2) may be expressed in terms of its Green's function by

$$\psi(\mathbf{r}) = -\int \xi(\mathbf{r}')G(\mathbf{r}\,|\,\mathbf{r}')\,d\mathbf{r}' \tag{6}$$

where $\mathbf{r}=x\mathbf{i}+y\mathbf{j}$, $\mathbf{r}'=x'\mathbf{i}+y'\mathbf{j}$, and

$$G(\mathbf{r}\,|\,\mathbf{r}')=(2\pi)^{-1}\{\log|\mathbf{r}-\mathbf{r}'|-\log|\mathbf{r}-\mathbf{r}^*|\} \tag{7}$$

with $\mathbf{r}^*=x'\mathbf{i}-y'\mathbf{j}$, so $\mathbf{r}^*$ is the reflection of $\mathbf{r}'$ across the boundary $y=0$ where we require $G(\mathbf{r}\,|\,\mathbf{r}')$ to satisfy condition (4).

The discretization of vorticity $\xi(\mathbf{r})$ can be effected by considering it to result from a distribution of point vortices located at positions $\{r_j\}$ each with vorticity $\xi_j=\Gamma_j\delta(\mathbf{r}_j-\mathbf{r})$; Γ_j is the circulation of the jth vortex, δ is the Dirac δ-function. We can write

$$\xi(\mathbf{r}')=\sum_j \Gamma_j\,\delta(\mathbf{r}_j-\mathbf{r}') \tag{8}$$

and substitute this expression into equation (6). Through equation (3) we can obtain an expression for the velocity field induced by $\xi(\mathbf{r})$ directly in terms of summations over the discrete vortices. This formulation of the discrete problem does not usually provide stable

solutions in regions of high vorticity because at small separation the interaction implied by (7) and (8) becomes singular. The Green's function (7) may be modified to suppress this singularity by considering a form

$$G(\mathbf{r} \mid \mathbf{r}') = \begin{cases} (2\pi)^{-1}\{\log|\mathbf{r}-\mathbf{r}'| - \log|\mathbf{r}-\mathbf{r}^*|\} & |\mathbf{r}-\mathbf{r}'| \geqslant \sigma \\ (2\pi\sigma)^{-1}\{|\mathbf{r}-\mathbf{r}'| - |\mathbf{r}-\mathbf{r}^*|\} & |\mathbf{r}-\mathbf{r}'| < \sigma \end{cases} \tag{9}$$

where σ is some appropriate core size to be determined. Leonard[10] describes alternative modifications which achieve a similar result.

This effectively provides an algorithm which can determine a velocity field $\mathbf{u}_\xi(\mathbf{r})$ induced at a point $\mathbf{r}$ by a collection of discrete vortices $\{\xi_j\}$. These vortices will convect in a superposition of this field together with the potential field $\mathbf{u}_\varphi$. In Reference 4 it is shown how a potential field may be computed to impose condition (4) at the obstacle, i.e. we require

$$\mathbf{u} \cdot \mathbf{n} = (\mathbf{u}_\xi + \mathbf{u}_\varphi) \cdot \mathbf{n} = 0 \tag{10}$$

at the solid boundary of the obstacle. Again the method of images can be invoked to represent the velocity potential φ (with $\mathbf{u}_\varphi = \operatorname{grad} \varphi$) in terms of a Green's function

$$\varphi(\mathbf{r}) = \oint \gamma(\mathbf{r}') G(\mathbf{r} \mid \mathbf{r}')\, \mathrm{d}\mathbf{r}' \tag{11}$$

This line integration is taken over the perimeter of the obstacle together with its mirror image in $y<0$; in principle any two-dimensional geometry can be accommodated by this procedure. The function $\gamma(\mathbf{r}')$ is an unknown source distribution and substitution of $\mathbf{u}_\varphi$ into (10) leads to an integral equation which may be discretized and cast into matrix form

$$\mathbf{A} \cdot \boldsymbol{\gamma} = \mathbf{b} \tag{12}$$

The column vector $\mathbf{b}$ is $2\mathbf{u}_\xi \cdot \mathbf{n}$ evaluated along the boundary. The matrix $\mathbf{A}$ is a function only of the geometry of the obstacle and of the irrotational flow field. This implies that $\mathbf{A}$ need only be inverted once at the outset of the calculation. Thus, at a given timestep we solve (12) for $\boldsymbol{\gamma}$ and hence evaluate $\mathbf{u}_\varphi$ from the grad operating on φ expressed by (11). In a time interval $\mathrm{d}t$, the displacements $(\mathrm{d}x_j, \mathrm{d}y_j)$ of the jth discrete vortex ξ_j are hence given by

$$\mathrm{d}x_j = \{u_\varphi(\mathbf{r}_j) + u_\xi(\mathbf{r}_j)\}\, \mathrm{d}t + \eta_x$$
$$\mathrm{d}y_j = \{v_\varphi(\mathbf{r}_j) + v_\xi(\mathbf{r}_j)\}\, \mathrm{d}t + \eta_y$$

where (η_x, η_y) is the diffusive random displacement we have described previously.

The random vortex method aims to simulate completely the physics of incompressible flow at high Reynolds number. To complete the simulation it remains to describe the mechanism of vortex generation at the solid boundary of the obstacle. The details of this are described in Reference 5. It will be noted that the flow field $\mathbf{u} = \mathbf{u}_\xi + \mathbf{u}_\varphi$ does not as yet satisfy the no-slip condition (5). We may imagine the formation of a shear layer parallel to the surface of the obstacle. This will be comprised of vortex sheets (which we discretize into sheet segments) which are of sufficient intensity and distribution to satisfy condition (5) at each point of the surface. As time progresses the diffusion and convection of these segments into the flow creates a boundary layer. Vorticity in this layer is assumed to satisfy the Prandtl boundary layer equations. When vortex sheets of intensity κ_j and sheet length h leave the boundary layer into the flow beyond, they become the discrete vortices ξ_j we have previously discussed, with $\xi_j = h\kappa_j$. If a core size of $\sigma = h/\pi$ is chosen in equation (9), then near the interface between the boundary layer and the external flow, the interaction of the vortex

sheets $\{\kappa_j\}$ approximates the interaction of the discrete point vortices $\{\xi_j\}$ (see Reference 12 for details).

The method we have described can provide a solution for the time-evolutionary laminar flow of wind over a two-dimensional building of arbitrary shape in cross-section. The method is computationally efficient and good agreement with experiment has been reported in other engineering contexts.[12] Unfortunately the extension of this method to three dimensional building shapes does not seem to be a trivial one, although some three-dimensional applications of the method have been reported in other aerodynamic contexts.[6,10] A mathematical discussion of the 'inviscid error' of the method is provided by Leonard.[10] There has been some suggestion[6] that turbulent effects can be observed in random vortex solutions, although such effects may be submerged by the grain of the vortex discretization. The method does not require *a priori* knowledge of the location of flow separation points—these arise naturally out of the solution procedure. In this respect the method would seem to offer some advantage over various other discrete vortex methods which have been reported (e.g. see References 13 and 14).

A control volume method

There are a number of ways of constructing the finite-difference analogue to the Navier–Stokes equation; although it may be shown that the different approaches to this problem are equivalent[15] they may exhibit quite different qualities so far as computational efficiency and stability are concerned. The control-volume approach has provided efficient and stable solutions for a wide range of problems. The particular control volume method we adopt is that described by Caretto *et al.*,[9] the method and its antecedents have been applied to problems characterized by high Reynolds number and the effect of Reynolds number and mesh size on such solutions has also been documented (e.g. Reference 7).

The method owes something of its stability to the fact that it does not derive directly from the continuum differential equations themselves, but from the macroscopic conservation laws which give rise to these equations.[15] We shall consider the case of a steady-state flow field, i.e. $\partial u/\partial t = 0$. The fluid space is divided into cells (in three dimensions these are 'control volumes') and around the perimeter of each cell we require that the *net* rate of convective plus diffusive inflow of momentum per unit volume vanish when this is added to the momentum sources internal to the cell.

We consider the flow of an incompressible fluid of uniform density ρ so that the momentum balance can be expressed (in continuum form) for the x-direction as

$$\rho\left\{u\frac{\partial u}{\partial x}+v\frac{\partial u}{\partial y}\right\}-\mu\left\{\frac{\partial^2 u}{\partial x^2}+\frac{\partial^2 u}{\partial y^2}\right\}+Q=0 \tag{13}$$

where μ is the viscosity of air; Q represents the source terms to be associated with the horizontal velocity component u (these consist of the pressure gradient $\partial p/\partial x$, and in regions of fluid adjacent to a solid boundary a shear stress term is also present). Corresponding to (13) there also exists a similar equation for the vertical velocity component, v.

The fluid is divided into control cells by a set of grid lines as depicted in Figure 1. The variables to be associated with the ith cell (central in Figure 1) are the velocity components (u_i, v_i) and the pressure p_i. For convenience in computing intercell mass fluxes and pressure gradients, the velocity components are taken to be those at the mid-point of the cell edges whereas the pressure is evaluated at the central 'node' of each cell. This results in a grid system which is staggered. We use the convention that the velocity components to be

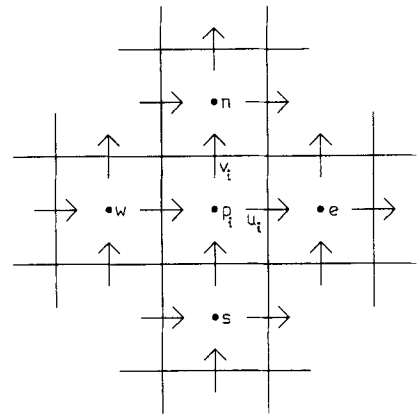

Figure 1. Grid arrangement for control volume method

associated with the ith cell are located between the cell and its neighbours to the east and north: thus in subsequent notation u_i and v_i are to be understood as equivalent to u_e and v_n respectively.

The method consists of two nested iterations. Prior to the first iteration an initial guess at the velocity field and pressure fields is made which should satisfy mass conservation but which is otherwise arbitrary. (Such an initial field can be determined from a potential flow calculation.) Thus at the start of each 'outer' iteration a velocity field exists which satisfies continuity (either from a previous 'inner' iteration, or from the initial guess), but this field does not in general satisfy momentum conservation. Horizontal momentum conservation at the ith control cell in relation to its four neighbours (labelled e, w, n, s in Figure 1) can be expressed

$$u_i\left\{\sum_j (\text{mass outflow from } i \text{ to } j) + Q_\tau\right\} = \sum_i \{(\text{mass inflow from } j \text{ to } i)u_j\} + Q_p \qquad (14)$$

where the summation is taken over $j \in \{e, w, n, s\}$. The terms Q_τ and Q_p represent, respectively, the source terms for wall shear stress and pressure forces. Since the velocity field satisfies continuity, i.e. since

$$\sum_j (\text{outflow from } i \text{ to } j) = \sum_i (\text{inflow from } j \text{ to } i) \qquad (15)$$

then equation (14) can be rearranged to obtain an expression for an intermediate velocity $\hat{u}_i$ where

$$\hat{u}_i = \left\{\sum_i a_i u_j + Q_p\right\} \Big/ \left\{\sum_j a_j + Q_\tau\right\} \qquad (16)$$

where we have followed Reference 8 in defining local transport coefficients $\{a_j\}$ by

$$a_j = \rho S_j\{\mu/d_j + \max(0, (-1)^m q_j)\} \qquad (17)$$

In (17) q_j is either u_j or v_i depending upon whether the jth neighbour cell is horizontally or vertically situated with respect to the ith cell. The factors S_j, etc. are the surface 'areas' of the various control volume faces (or in our two-dimensional case, the 'lengths' of the control cell edges), and d_j is the distance between adjacent cell nodes. The first term in the square

brackets represents a diffusive contribution and the second is a convective 'upwind' contribution. (The index m in (17) is an odd integer when $j \in \{e, n\}$ and even when $j \in \{w, s\}$.)

Equation (16) represents a linear approximation to the momentum transport equation for u. The non-linear effects of the convective terms are introduced by iteration of (16) using updated values of velocity fields and source terms. However the $(\hat{u}_i, \hat{v}_i)$ values cannot be used directly as input to the next iteration, since they do not in general satisfy the continuity condition, which requires that the sum of inward convective mass fluxes to each cell must vanish; this can be expressed as

$$\sum_j \hat{c}_j = 0 \tag{18}$$

where we define $\hat{c}_j = (-1)^m \rho S_j \hat{q}_j$. If (18) is not satisfied for a given 'outer' iterate $(\hat{u}_i, \hat{v}_i)$, then balance may be restored (following Reference 9) by computing a pressure increment $\mathrm{d}p_i$ such that

$$c_j = \hat{c}_j + \frac{\partial \hat{c}_j}{\partial p}(\mathrm{d}p_i - \mathrm{d}p_j) \tag{19}$$

where $\sum_j c_j = 0$, and the partial derivatives $\partial \hat{c}_j / \partial p$ are determined from the intermediate velocity field by

$$\frac{\partial \hat{c}_j}{\partial p} = \rho S_j \frac{\partial \hat{q}_j}{\partial p}$$

If the pressure source is expressed as $Q_p = S_j(p_i - p_j)$ then equation (16) implies that

$$\frac{\partial \hat{c}_j}{\partial p} = \rho S_j^2 \Big/ \left\{ \sum_{j'} a_{j'} + Q_\tau \right\} \tag{20}$$

Combining equations (18) and (19) leads to the finite difference analogue of a Poisson's equation for $\mathrm{d}p_i$,

$$\mathrm{d}p_i = \sum_j \left\{ \frac{\partial \hat{c}_j}{\partial p} \mathrm{d}p_j + \hat{c}_j \right\} \Big/ \sum_j \frac{\partial \hat{c}_j}{\partial p} \tag{21}$$

This equation may be solved by various iterative methods.[15] We chose to use a successive over-relaxation method because of the ease with which arbitrarily shaped boundaries may be handled. In addition, it may be shown that $\partial \hat{c}_i / \partial p$ and Q_τ are strictly non-negative so equation (21) possesses weak diagonal dominance: this ensures that a successive over-relaxation iteration scheme will be convergent.

Solution of (21) constitutes the 'inner' iteration of our algorithm. After a converged solution to (21) is obtained during the kth 'outer' iteration, the velocity and pressure fields are updated to satisfy continuity through

$$q_i^k = c_i / \rho S_i$$
$$p_i^k = p_i^{k-1} + \mathrm{d}p_i$$

These velocity and pressure fields (which will now no longer in general satisfy momentum conservation) may be substituted back into equation (16) and the 'outer' iteration repeated. The whole nested procedure is repeated until both momentum conservation and the continuity condition are simultaneously satisfied to a specified level of accuracy. The method used for the outer iteration should be one which preserves the continuity-satisfying velocity field while the intermediate field is computed. We have therefore adopted a scheme based on

simple Jacobi iteration which, despite its relatively slow convergence rate, is simple to implement for irregular boundaries.

The method we have just described is extremely versatile and robust. In addition to the problem we have posed, more complicated problems can be treated involving body forces, such as buoyancy, and the effects of heat transfer; semi-empirical turbulence models can be introduced directly into the algorithm. There is considerable flexibility in the geometry of boundaries which can be considered. From the point of view of architectural problems, perhaps the most crucial attribute is the ease with which this method extends into three dimensions.

SOME EXAMPLES OF NUMERICAL FLOW SIMULATION

To illustrate both methods we consider wind flow over a two-dimensional structure with a symmetrical roof of arbitrary pitch. Such a pitched roof is obviously a common building form and has been the subject of considerable experimental study. Since it is a bluff body of some geometrical complexity, it can illustrate the various advantages of the particular methods we have adopted.

Application of the random vortex method

We intend to compute solutions to the Navier–Stokes equation (1) in terms of the dimensionless variables $\mathbf{u}$, $\mathbf{r}$, and t, which can be transformed into dimensional variables in the usual way by specifying a standard scale length L and scale velocity U. Thus dimensional variables $\tilde{\mathbf{u}}$, $\tilde{\mathbf{r}}$, and $\tilde{t}$ may be determined from

$$\tilde{\mathbf{u}} = \mathbf{u}U; \qquad \tilde{\mathbf{r}} = \mathbf{r}L; \qquad \tilde{t} = tT$$

with $T = L/U$. For architectural problems L may be chosen to be the building height and U the free-stream velocity at the ridge height; typical values of these scale parameters might be $U = 2{\cdot}5$ m/s, $L = 10$ m; hence $T = 4$ s.

The geometry of the pitched roof obstacle explicitly enters through the potential flow calculation since the line-integration (11) is taken over the perimeter of the building in section (together with its contiguous mirror image across $y = 0$). Discrete expression may be given to this geometry by defining a collection of 'body points' along this perimeter dividing it into linear increments. At each body point we also require to know $\mathbf{n}$ and $\mathbf{s}$, the unit vectors normal and tangential to the building surface. Also, a boundary layer region is defined along the surface, some standard deviations thick; a mirror image of this layer 'below' the surface of the building is also defined.

In constructing the potential flow $\mathbf{u}_\varphi$ some description of the atmospheric boundary layer is desired. To do this it is assumed that the wind in the absence of the building (i.e. the free-stream wind) flows horizontally with a vertical profile given by

$$u(y) = u(y_g)[y/y_g]^\alpha \tag{22}$$

The height to the top of the boundary layer—i.e. the gradient height, y_g—is taken to be 20 units; the exponent $\alpha = 0{\cdot}29$ corresponds to a profile associated with a suburban environment. The wind speed at $y = y_g$ is taken to be 4 dimensionless units. The free-stream velocity is to be considered implicit in the notation $\mathbf{u}_\xi(\mathbf{r})$.

It is assumed that a wind with this prescribed profile will start up impulsively at $t = 0$. At this first time-step there are no discrete vortices yet in the flow and $\mathbf{u}_\xi$ consists entirely of the

free-stream velocity field. The potential flow is calculated such that (4) is satisfied on the surface of the building: the sum $\mathbf{u}_\xi + \mathbf{u}_\varphi$ corresponds to the flow field in the absence of the viscous effects of the obstacle. In order to impose the no-slip condition (5) a distribution of vortex sheet segments are entered into the flow at each body point; these diffuse by a random displacement (η_x, η_y) normal to the building surface. At subsequent time-steps $\mathbf{u}_\xi$ will also include a velocity component induced by the pre-existent vortex sheets. Otherwise the calculation proceeds as in the first time-step. A new set of vortex sheets is created at the body points and these diffuse into the boundary layer: the sheets created in previous time-steps convect in the local velocity field as well as diffusing.

The success of the random vortex method depends upon an accurate representation of the boundary layer; the detailed description of this is to be found in Reference 5. When the sheets leave the boundary layer into the flow beyond, they become discrete 'point' vortices interacting with each other according to (9). If the sheets migrate into the image boundary layer, they are reflected back out into the boundary layer proper. If the sheets pass into the deeper interior of the building, they are removed from the flow calculation. Similarly, if they pass into the region $y<0$, or pass beyond the region of interest (i.e. if they convect sufficiently far downstream so that they retain relatively little influence over the flow near the building) then these too are removed from the calculation.

Figure 2 illustrates streak-line diagrams for a typical flow solution. The Reynolds number of this flow is $Re = 10^6$; the ridge height of the building is 1 unit, the pitch is 45°. The building geometry is numerically specified by 40 body points. The discrete vortices are removed from the computation after they have convected a distance greater than 8 dimensionless units downstream.

The six frames of Figure 2 illustrate equally-spaced excerpts from the first 80 timesteps after flow initialization: each timestep is 0·02 dimensionless units in duration, so the full 80 steps correspond to 6·4 s if $T = 4$ s. Each streak in frame 1 represents the three timesteps 12 to 14: by timestep 14 there are 185 discrete vortex elements entered into the flow. Similarly in frame 2, steps 24 to 26 are represented (with 243 vortex elements); frame 3, steps 36 to 38 (290 vortex elements); frame 4, steps 48 to 50 (328 vortex elements); frame 5, steps 60 to 62 (346 vortex elements); frame 6, steps 72 to 74 (408 vortex elements).

In the first frame of Figure 2 a separation zone may be seen to develop at the leeward roof. A recirculation eddy forms in this zone: in frames 2–6 this eddy detaches itself from the building and forms the downstream wake. Eventually it is washed out of the solution, while a new eddy is formed at the roof. The process is repeated and there ensues a sequence of vortex shedding at the roof. Because of its impulsive character, the recirculation eddy associated with the initial conditions is probably anomalous, but as time progresses the shedding sequence becomes increasingly regular.

Figure 3 illustrates the flow later in its development, between timesteps 320 and 400. Each streak in frame 1 of Figure 3 represents timesteps 332 to 334, with 860 discrete vortices entered in the flow; frame 6 represents steps 392 to 394 with 885 discrete vortices in the flow. One may observe in Figure 3 an eddy sequence. The Strouhal number determined from the first four eddies in this simulation is approximately 0·3 (taking the ridge height of the building to be the wake width, and the characteristic velocity to be the free-stream at the ridge). The 'dimensional' shedding frequency associated with Figures 2 and 3 will be proportional to T^{-1}, and hence to U (if L is kept constant). This is consistent with experimental observations.[16] Figures 2 and 3 bear an interesting comparision with well-known water-tunnel photographs (e.g. see plate 9 in Reference 17).

The fact that time-evolutionary solutions are obtained from this method suggests that it

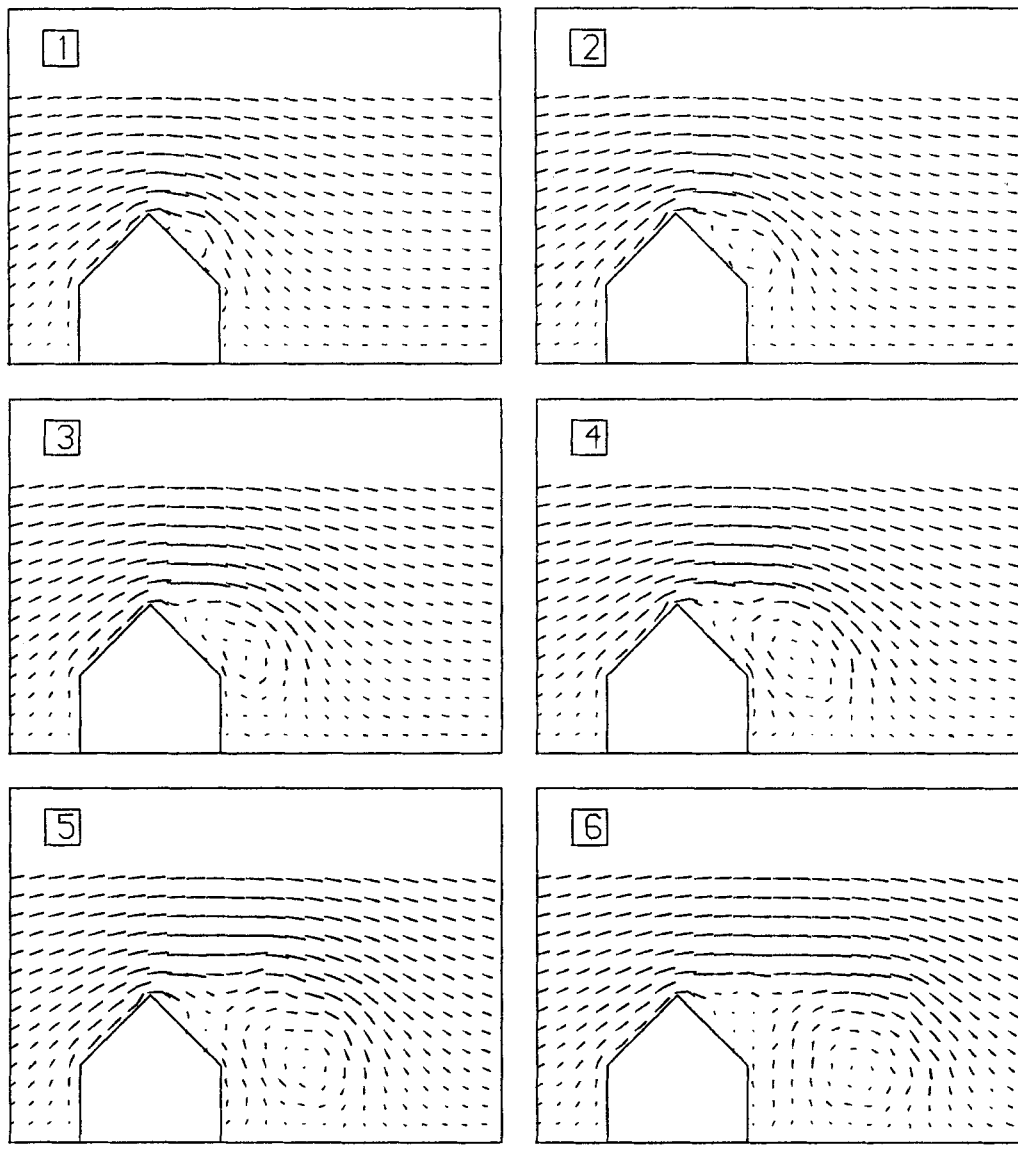

Figure 2. Evolution over first 80 timesteps after flow initialization; this represents a total time interval of 1·6 dimensionless units

may be suited to studying impulsive phenomena such as wind gusting. After sufficient time has elapsed and a quasi-periodic flow sequence is achieved, then the inlet boundary profile can be adjusted at will in the time-domain to exhibit a prescribed time variation. The effect of this on the flow can then be monitored.

In applications of studies of the wind environment of buildings it is often most useful to consider time-averaged flows. Field anemometers typically have a high-frequency cut-off of several seconds. To evaluate mean fields using the random vortex method, one must average over a sufficiently large number of timesteps. Figure 4 illustrates the flow averaged over timesteps 3 to 100 (an interval of 8 s if $T = 4$ s). The average pressure distribution has also

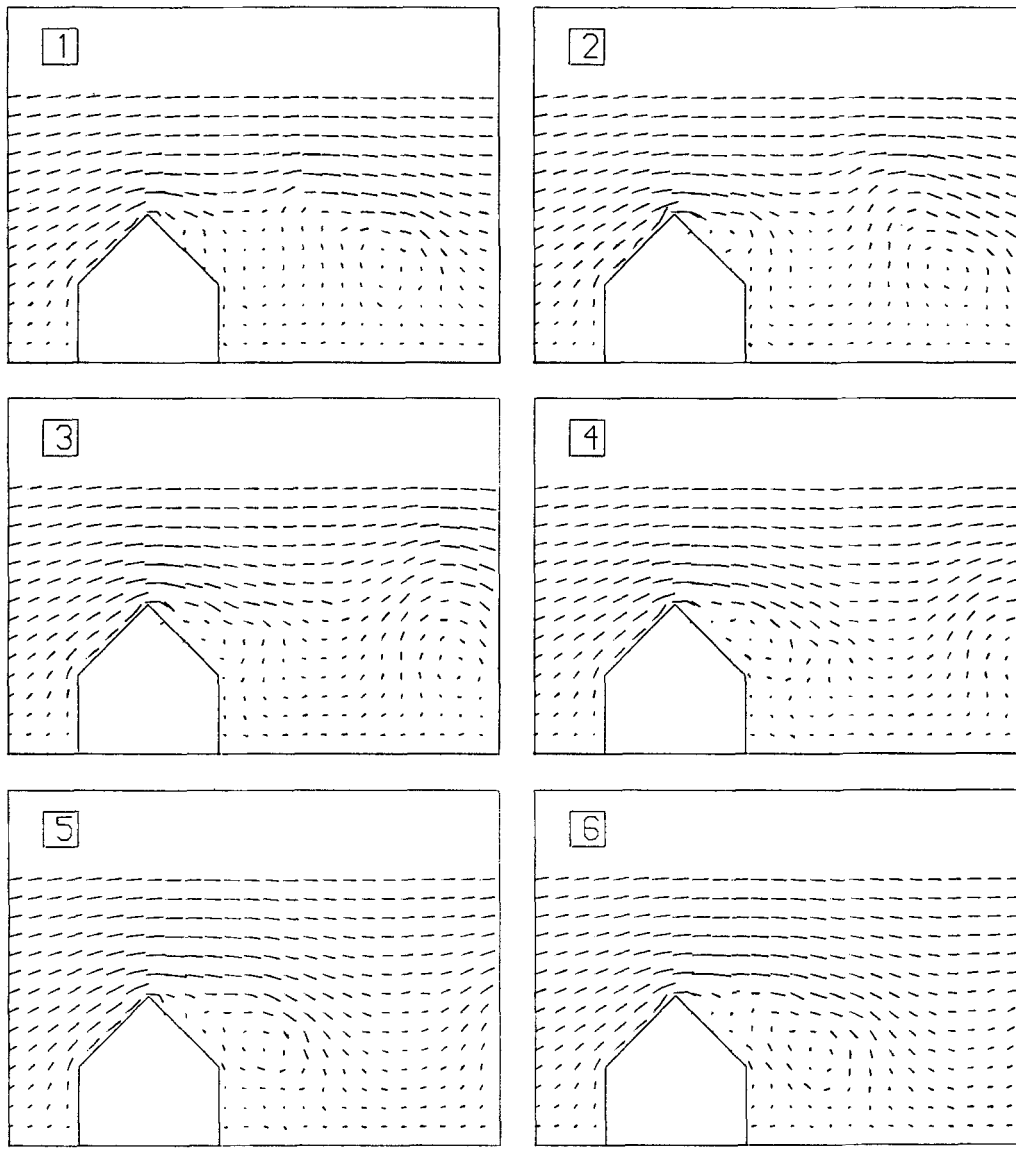

Figure 3. Evolution between timesteps 320 and 400

been evaluated over the building perimeter, along with the standard deviation of this pressure over the averaging time-interval. (Second-order one-sided differences are applied to $\mathbf{u}$ in order to evaluate grad p from the Navier–Stokes equation; then the tangential component of this gradient is integrated at each point of the building surface to obtain a 'relative pressure'.) This pressure distribution may be used as a check on the plausibility of solutions, since the pressure distribution on the roof is a sensitive function of pitch angle. A negative value of pressure indicates suction with respect to the building surface. These numerical computations show general qualitative agreement to experiment, although a serious attempt has not yet been made to compare these numerical solutions in detail with wind-tunnel measurements.

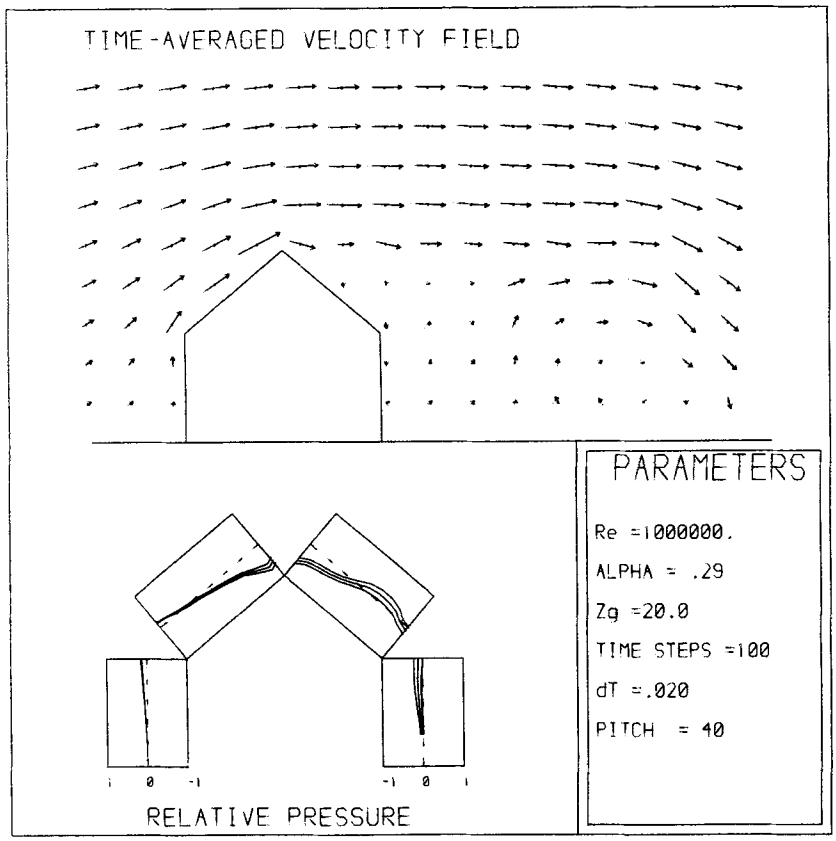

Figure 4. Velocity field averaged over first 100 timesteps; mean relative pressure over the building surface and its standard deviation

A reliable numerical calculation of the pressure gradient at the surface of a building would have obvious application to the problem of structural loading. The solutions to the random vortex method may well achieve sufficient accuracy for this: Cheer[12] has reported solutions for the drag on a cylinder which show agreement with wind tunnel experiment within 2 per cent. Before the numerical calculations we have presented can be used with any reliability for structural applications they must be compared in detail with corresponding wind tunnel measurements and to site measurements (e.g. Reference 18).

The calculation of the mean field illustrated in Figure 4 required some 26 minutes cpu on a DEC System 10 computer; an ultimate 500 vortex elements required 120 Kbytes of storage. If the averaging procedure were continued over a statistically significant number of shedding cycles, then a steady state of the solution could be approached. Despite the conceptual attractions (as advocated by Roache[15]) of using a time-dependent method to determine a mean flow, this route proves uneconomic for our purpose. We use a stationary technique—the control volume method—to evaluate the steady flow field.

Application of the control volume method

Wind tunnel models of airflow around buildings exploit the fact that the wind separates at fixed positions, usually at the sharp edges of the obstacle. This implies that indicators of the

structure of the flow (e.g. the Strouhal frequency) can be largely independent of Reynolds number.[16] The simplified scaling procedures adequate to such modelling are discussed in Reference 1. (In the case of flow separation from a curved solid surface, such a simplified scaling procedure is not necessarily valid, since the flow may be strongly dependent on Reynolds number.) There is some analogy with this to be found in the problem of the numerical computation of flow over an obstacle with sharp edges, when control volume methods are used. If the separation points are fixed at the corners of a building, then it may be possible to determine numerically the gross features of the flow without high resolution of the boundary layer.

Problems of high Reynolds number are characterized by turbulence; if the turbulence is homogeneous and isotropic, a crude approximation of turbulent effects may be achieved by increasing the laminar viscosity by some constant factor which may be determined by comparing computed solutions to real, well-defined flow patterns. Thus we may postulate an effective turbulent or 'eddy' viscosity to be

$$\mu_{\text{effective}} = f\mu_{\text{laminar}} \tag{23}$$

where typically $f > 1000$.

The crudeness of such an approximation is not really satisfactory for flow which is recirculating. A more appropriate model would require the addition of at least two turbulence transport equations. Semi-empirical models of turbulence such as the k–ε model can be incorporated into control volume methods.[19] Such models require knowledge of prescribed turbulence variables associated with the inlet profile (i.e. the turbulent kinetic energy per unit mass and its rate of dissipation). These variables must be specified in such a way that they reproduce the characteristics of measured wind turbulence (in particular, the turbulence intensity and its power spectrum.[20]) We have not yet devised a satisfactory method of doing this and we resort instead to equation (23).

The effect of non-rectangular boundaries is simulated by adjusting the surface areas of cell faces which are cut by grid lines. Thus cells which are totally embedded in an obstacle have all their areas set to zero; partially blocked cells have each of their areas set individually according to the local grid-obstacle geometry. Despite the coarseness of this boundary representation it has considerable computational advantages, since the appearance of the cell areas in many of the algorithm equations permits use of these equations both within the bulk fluid and at boundaries.

The shear stress term to be included in equation (16) near solid boundaries may be computed to an accuracy sufficient for our purposes by application of the Blasius formula for turbulent flow over a flat plate, which may be expressed as

$$\tau = 0{\cdot}03 Re^{-0{\cdot}2} \rho u^2$$

where u is the velocity parallel to the surface at the outer edge of the boundary layer, and Re is a Reynolds number based on a typical building dimension. Thus we have, for cells adjacent to a solid boundary

$$Q_\tau = \tau B_i / |u_i| = 0{\cdot}03 Re^{-0{\cdot}2} \rho \, |u_i| \, B_i$$

where B_i represents the occluded area (or length) of a cell face in the direction parallel to u.

The free boundaries of the flow are assumed to be undisturbed by the presence of the building: the inlet (and outlet) profile is that expressed by equation (22).

The convergence of the momentum calculation is observed at each iteration through the residuals R where at the kth iteration

$$R_u^k = \max_i |(u_i^k - u_i^{k-1})/u_i^k|$$

Here we additionally require $u_i^k > u_{\min}$ to exclude very small values of u_i^k in the denominator. A pressure residual is also computed,

$$R_p^k = \max_i |\mathrm{d}p_i/p_i|$$

Convergence is achieved when velocity and pressure residuals are simultaneously less than some prescribed small number. For each iteration of the momentum equation it is required to solve iteratively the Poisson equation (21). The convergence criteria for these 'inner' iterations may be related indirectly to the degree of continuity error associated with the external momentum calculation.

Figure 5(a) displays a grid distribution which was used to compute the steady-state flow around a building form with roof pitch 30°. A variable grid was chosen so that regions far from the building may be more coarsely represented in order to reduce the size of computation. The smallest cells are 1 m square so no attempt is made to resolve the surface boundary layer.

The inlet flow is specified as a 'rural' boundary layer, i.e. $u(y)$ is given by equation (22) with an exponent of $\alpha = 0{\cdot}16$, and $y_g = 275$ m. The reference value of u at $y_g = 10$ m is set to 5 m/s. The building width is 8 m and its ridge height is 6·3 m.

A streak-line diagram of the computed steady flow is illustrated in Figure 5(b). Each streak represents the motion of a particle embedded in the flow over a short time interval (1 s), thus the streak length is proportional to local velocity. The principal features of the mean flow are seen to be the sharp separation at the ridge with subsequent reattachment of the separated layer some 60 m downstream. The inclusion of the reattachment zone in the solution domain makes convergence of the solution fairly slow, but it is essential if the leeward recirculation zone is to be properly represented. The corresponding pressure distribution is shown in Figure 5(c), in which the value at the origin has been arbitrarily set to zero. The high pressure at the windward stagnation point and the low pressure region corresponding to the leeward recirculation are also to be seen in the solution.

Solution of this problem to obtain residuals less than 0·05 took four minutes to compute on a DEC System 10. The number of cells in the grid was 902 which gave rise to a total core requirement of about 85 Kbytes.

It should be emphasized that Figures 4 and 5 are not directly comparable; Figure 4 represents an average over 8 s of the flow development, whereas Figure 5 is a solution of the steady equation. In principle, the vortex method could be run for much longer periods and it could be expected that a steady time-averaged flow field would be obtained. As noted previously, this would not be economical for our purpose; the vortex method is more suited in the present application to elucidating the time-dependence of the flow solution.

CONCLUSIONS

The numerical solutions illustrated in the last section were calculated using computer programs of modest core and time requirements. These programs could be run on a mini-computer and, in principle, they could provide a basis for an efficient design tool.

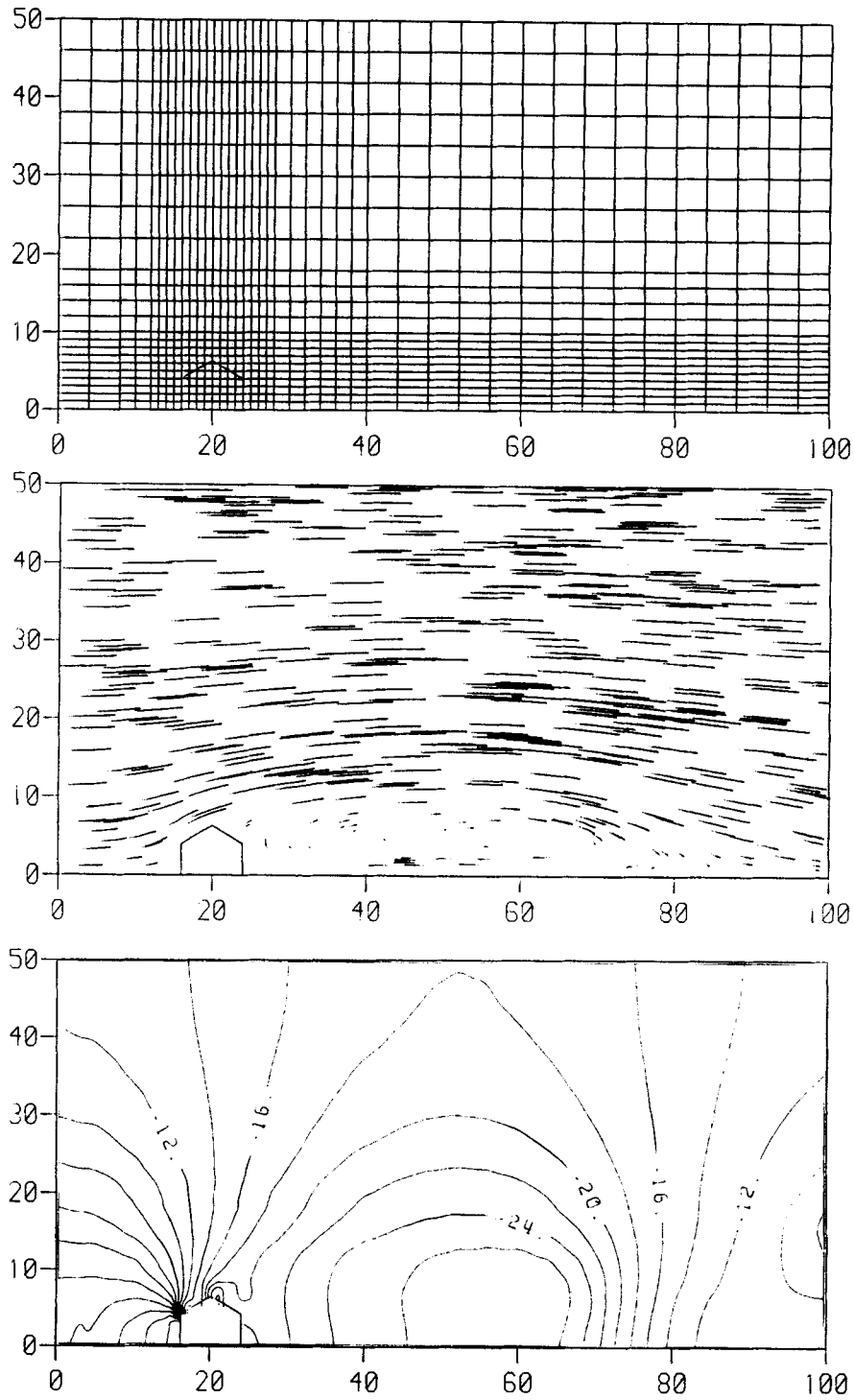

Figure 5. Example of control volume method applied to building with roof pitch of 30°: (a) grid distribution; (b) streakline plot; (c) global pressure contours (SI units)

Of course, such two-dimensional procedures as we have described can represent little more than a first step towards a simulation of flow around real buildings. Buildings are three-dimensional objects: their interaction with wind is strongly influenced by the wind's angle of incidence. If numerical modelling techniques are to be made comparable to wind-tunnel measurement, they must be able to represent the three-dimensionality of real wind flow. We are presently extending the control volume method into three dimensions. In the future it would be useful also to adopt a three-dimensional version of the random vortex method to treat wind-flow problems.

We have confined ourselves to a laminar approach to the problem. It is important now to introduce into the modelling some more adequate representation of the turbulence of real situations. Within the literature of turbulence theory there exists a number of specific modelling possibilities (these essentially corresponding to different closure conditions). However, it remains to be decided which of these best corresponds to the turbulence content of a building's wind environment.

In principle the methods we discuss can accommodate complex building forms. So far as the vortex method is concerned, the shape of the building is numerically specified and is quite arbitrary. The control volume method is particularly suited to forms with sharp edges—a building category which includes most forms of interest. (We note also that both methods can in principle treat the case of a building raised on pilotti).

We are especially interested to investigate numerically the question of how one building may affect the wind environment of another. We have already applied the numerical methods described in this paper to a simple configuration of two buildings.[21] We hope that the relative ease with which numerical experiments can be performed on a computer may eventually make possible the systematic morphological study of a large number of different building shapes and configurations.

ACKNOWLEDGEMENTS

This work is supported by the U.K. SERC (grants GR/A/8632·9 and GR/B/92201). The authors thank the members of EdCAAD and Dr. F. Smith for their respective contributions to this project.

REFERENCES

1. T. V. Lawson, 'The wind environment of buildings. A logical establishment of criteria', *Report TVL/730*, University of Bristol, Department of Aeronautical Engineering, 1973.
2. P. M. Jones and C. B. Wilson, 'Wind flow in an urban area: comparison of full scale and model flows', *Build. Sci.*, **3,** 31–40 (1968).
3. R. C. F. Dye, 'Comparison of full-scale and wind-tunnel model measurements of ground winds around a tower building', *J. Wind Eng. Ind. Aerodyn.*, **6,** 311–326 (1980).
4. A. J. Chorin, 'Numerical study of slightly viscous flow', *J. Fluid Mech.*, **57,** 785–796 (1973).
5. A. J. Chorin, 'Vortex sheet approximation of boundary layers' *J. Comput. Phys.*, **27,** 428–442 (1978).
6. A. J. Chorin, 'Vortex models and boundary layer instability', *SIAM J. Sci. Stat. Comput.*, **1,** 1–21 (1980).
7. A. K. Runchal, D. B. Spalding and M. Wolfshtein, 'Numerical solution of the elliptic equations for transport of vorticity, heat, and matter in two-dimensional flow', *Phys. Fluids*, Supp. 2, II21–II28 (1969).
8. L. S. Caretto, R. M. Curr and D. B. Spalding, 'Two numerical methods for three-dimensional boundary-layers', *Comput. Methods Appl. Mech. Eng.*, **1,** 39–57 (1972).
9. L. S. Caretto, A. D. Gosman, S. V. Patankar and D. B. Spalding, 'Two calculation procedures for steady, three-dimensional flows with recirculation', *Proc. 3rd Int. Conf. Num. Methods. Fluid Mech.*, 60–68, Springer Verlag, Berlin, 1972.
10. A. Leonard, 'Vortex methods for flow simulation', *J. Comput. Phys.*, **37,** 289–335 (1980).
11. D. J. Maull, 'An introduction to the discrete vortex method', *IUTAM/IAHR*, Karlsruhe (1979).
12. A. Y. L. Cheer, 'Numerical study of incompressible slightly viscous flow past blunt bodies and airfoils', *Ph.D. Thesis*, Lawrence Berkeley Laboratory, University of California, 1981.

13. R. I. Lewis, 'Surface vorticity modelling of separated flows from two-dimensional bluff bodies of aribitrary shape', *J. Mech. Eng. Sci.*, **23,** 1–12 (1981).
14. P. K. Stansby, 'A numerical study of vortex shedding from one and two circular cylinders', *Aeronaut. Q.*, **32,** 48–71 (1981).
15. P. J. Roache, *Computational Fluid Dynamics*, Hermosa Publishers, Albuquerque, N.M., 1976.
16. I. Grant and F. H. Barnes, 'The vortex shedding and drag associated with structural elements', *J. Wind. Eng. Ind. Aerodyn.* **8,** 115–122 (1981).
17. G. K. Batchelor, *An Introduction to Fluid Dynamics*, Cambridge University Press, 1967.
18. K. J. Eaton, J. R. Mayne, and N. J. Cook, 'Wind loads on low-rise buildings—effects of roof geometry', *BRE Current Paper CP1/76*, 1976.
19. B. E. Launder and D. B. Spalding, *Mathematical Models of Turbulence*, Academic Press, N.Y., 1972.
20. D. M. Deaves and R. I. Harris, 'A mathematical model of the structure of strong winds', *CIRIA, Report* 76, *London*, 1978.
21. T. Hanson, F. Smith, D. Summers and C. B. Wilson, 'Computer simulation of wind flow around buildings, *Comput. Aid. Des.*, **14,** 27–31 (1982).